Thrust Performance and Plasma Characteristics of Low Power Hall Thrusters

Hirokazu Tahara, Daisuke Goto, Toshiaki Yasui and Takao Yoshikawa
Division of Mechanical Science, Dept. of Systems and Human Science
Graduate School of Engineering Science, Osaka University
1-3, Machikaneyama, Toyonaka, Osaka 560-8531, Japan
+81-6-6850-6178
tahara@me.es.osaka-u.ac.jp

IEPC-01-042

Low-power Hall thruster performance was investigated using THT-series Hall thrusters. The THT-IIIA thruster could be stably operated in a wide range of magnetic field strength. A high thrust efficiency was achieved with a low discharge current and a high thrust for an optimum magnetic field strength regardless of discharge voltage at a constant mass flow rate. As a result, both the thrust and the specific impulse ranged from 10 to 70 mN and from 1200 to 2300 sec, respectively, at discharge voltages of 200-500 V with mass flow rates of 1-3 mg/s in a wide input power range of 250-1800 W. The thrust efficiency ranged from 30 to 45 %. Furthermore, one-dimensional flowfield calculation was made to understand the inner physical phenomena. Both ionization and plasma acceleration were found to efficiently occur in a thin region with a few mm thick near the acceleration channel exit. The calculated results roughly agreed with the experimental ones.

Introduction

The closed-electron-drift Hall-effect thruster is a promising propulsion device in space. The performance has been improved in Russia since 1960[1]. Because 1-2 kW class Hall thrusters can achieve the high performance of thrust 50-100 mN and thrust efficiency 40-50 % at specific impulses of 1000-2000 sec, they are expected to be used as main thrusters for near-earth missions in the United States and Europe[2],[3]. Even in Japan, the high performance attracts attention of mission planners[4]-[6]. However, the detailed physics on plasma characteristics and plasma acceleration processes is still unclear. We need both basic and practical studies in order to improve Hall thruster performance by understanding inner physical phenomena.

In Osaka University, an experimental facility was constructed in 1997 to study plasma acceleration processes and unstable operational phenomena in low power Hall thrusters and to evaluate contamination due to Hall thruster plumes[4],[5]. Preliminary experiments were made using THT-series low-power Hall thrusters to obtain fundamental Hall thruster operational characteristics. The influences of width and length of acceleration channel on thruster performance were mainly investigated[6]. The guideline of Hall thruster design was established on acceleration channel configuration.

In the present study, basic experiments are made using THT-III-series low-power Hall thrusters to examine stable operational conditions with varying discharge voltage, propellant mass flow rate, and magnetic field shape and strength. Furthermore, one-dimensional Hall thruster flowfield calculation, in which axial motion of ions; axial and azimuthal motions of electrons perpendicular to magnetic field are considered, is carried out to understand the plasma features and the plasma acceleration processes. The model includes first ionization by direct electron-neutral collisions, electron-neutral elastic collisions, electron-ion Coulomb collisions, Bohm diffusion (anomalous diffusion); channel wall losses of ion flux and electron energy with secondary electron emission effect.

Experimental Apparatus

The experimental facility, as shown in Fig.1, mainly consists of a water-cooled stainless steel vacuum tank 1.2 m in diameter x 2.25 m long, two compound turbo molecular pumps, several DC power supplies and a thrust measurement system[4]-[6]. The vacuum tank pressure is kept a range of 10^{-3}–10^{-4} Pa under operations. A clean and high vacuum environment can be created by using the oil-free turbo molecular pump system, which is useful to study contamination due to Hall thruster plumes.

* Presented as Paper IEPC-01-042 at the 27th International Electric Propulsion Conference, Pasadena, CA, 15-19 October,2001.

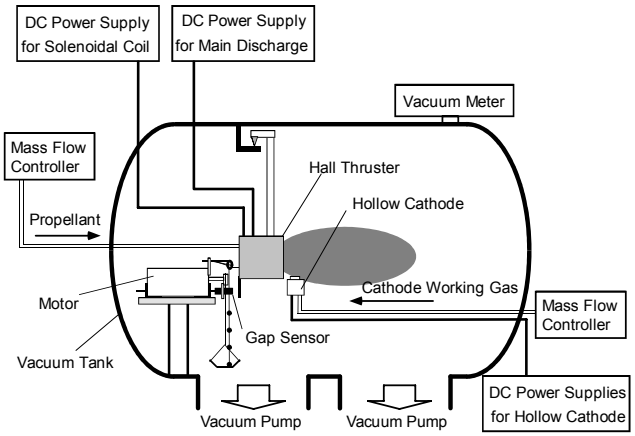

Figure 1 Experimental facility of Hall thruster.

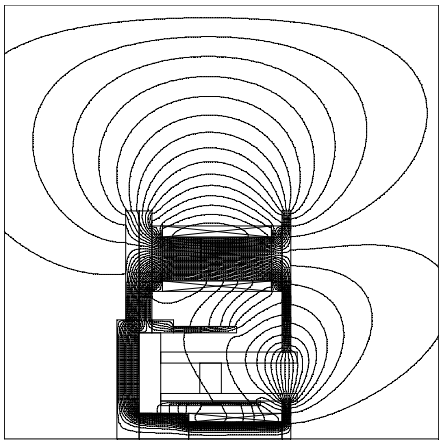

Figure 3 Magnetic field lines calculated for THT-IIIA thruster.

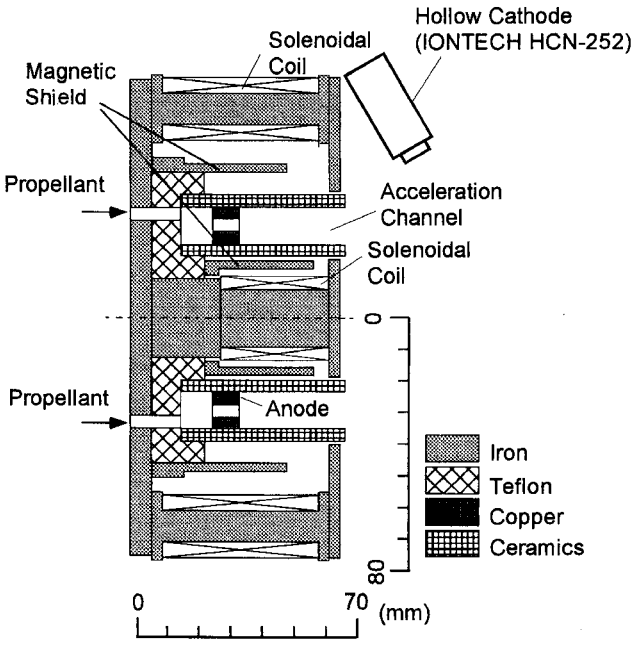

Figure 2 Configuration of THT-IIIA Hall thruster.

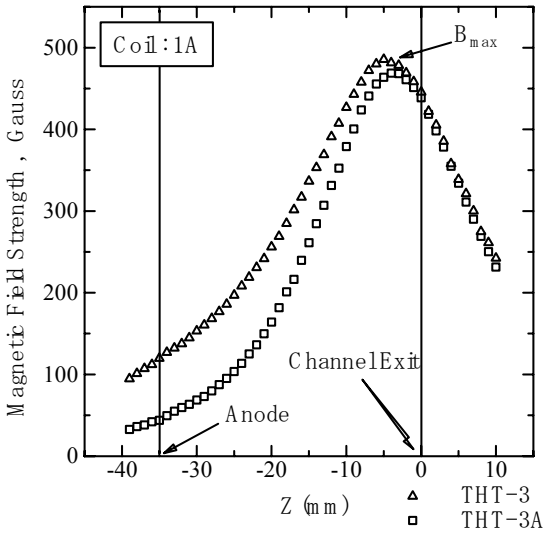

Figure 4 Radial magnetic field strength on radially intermediate region in acceleration channel of THT-III-series Hall thrusters at coil current of 1 A by Hall sensor measurement.

Thrusts are measured by a pendulum method, as shown in Fig.1. A Hall thruster is mounted on a thrust stand suspended with stainless wires, and the position of the thrust stand is detected by an eddy-current-type gap sensor (non-contacting micro-displacement meter). It has a high sensitivity and a good linearity. Thrust calibration is conducted with a weight and pulley arrangement which is able to apply a known force to the thrust stand under vacuum environment. With this design, friction force was small, and it resulted in no measurable hysteresis.

The THT-III-series thruster, as shown in Fig.2, has an acceleration channel of 35 mm in length and 14 mm in width, i.e., with an outer diameter of 70 mm and an inner diameter of 42 mm. The wall material of the acceleration channel is Boron Nitride (BN) ceramics. The anode is made of copper. A hollow cathode is used as the main cathode. After propellant gas is introduced from two lines into a plenum chamber behind the anode, it is uniformly injected from 24 ports azimuthally drilled on the anode into the acceleration channel.

The thruster has a main magnetic coil on the central axis and four magnetic coils on the radial outer side because of easy heat removal due to radiation. The thrusters without and with a magnetic shield are named THT-III and THT-IIIA,

respectively. Figure 3 shows the magnetic field lines calculated for the THT-IIIA thruster. Figure 4 shows the radial magnetic field strength on the radially intermediate region in the acceleration channel of the THT-III and THT-IIIA thrusters at a coil current of 1 A. They are measured with a Hall sensor. The magnetic field strength decreases as distance to the anode decreases, and it has a maximum near the channel exit and a minimum at the anode. The magnetic field strength for the THT-III thruster is higher than that for the THT-IIIA thruster inside the acceleration channel except for near the channel exit; it is about three times at the anode; in other words, the magnetic field for the THT-IIIA thruster is concentrated near the acceleration channel exit.

Xenon is used as the propellant. In a series of experiments, discharge currents and thrusts are measured as varying discharge voltage, mass flow rate and magnetic field strength and shape, and specific impulses and thrust efficiencies are evaluated.

One-Dimensional Flowfield Calculation

Hall thruster flowfield is calculated using a simple one-dimensional model, as shown in Fig.5, in which axial motion of ions; axial and azimuthal motions of electrons perpendicular to magnetic field are considered. The model includes first ionization by direct electron-neutral collisions, electron-neutral elastic collisions, electron-ion Coulomb collisions, Bohm diffusion (anomalous diffusion); channel wall losses of ion flux and electron energy with secondary electron emission effect, but without electron conduction enhanced near the channel wall. The present model is similar to Ahedo's[7],[8].

The following conservation equations of mass, axial momentum of ions, axial momentum of electrons considering a back electric field induced by azimuthal velocity x magnetic field, and energy of electrons are made.

Mass:

$$\frac{d}{dx}\left(N_e V_i\right) + N_e V_i \frac{1}{A}\frac{dA}{dx} = N_e\left(\nu_{ion} - \nu_{wall}\right) \tag{1}$$

where N_e is electron (ion) number density, V_i axial ion velocity, A cross sectional area of acceleration channel, ν_{ion} ionization collision frequency, and ν_{wall} frequency of ion flux loss to channel wall.

Ion momentum in axial direction:

$$M_i V_i \frac{dV_i}{dx} = -e\frac{d\phi}{dx} - M_i \nu_{ion}\left(V_i - V_n\right) + M_i \nu_{wall} V_i \tag{2}$$

where M_i is ion mass, e electron charge, ϕ electric potential, and V_n axial neutral velocity.

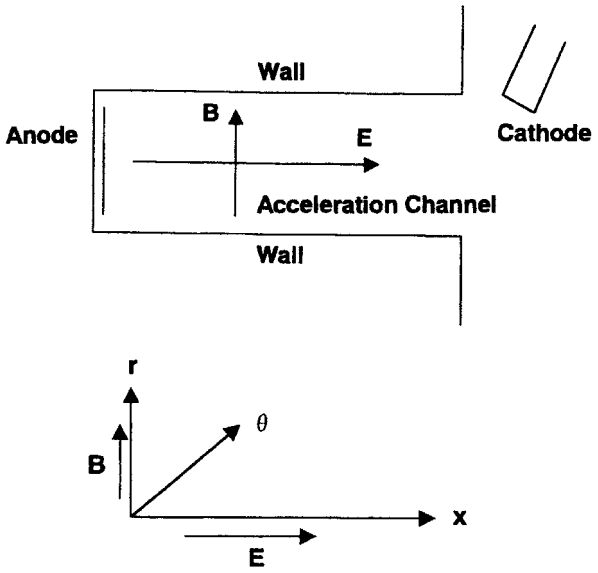

Figure 5 Calculation model of one-dimensional Hall thruster flowfield.

Electron momentum in axial direction:

$$\frac{k}{N_e}\frac{d}{dx}\left(N_e T_e\right) + kT_e \frac{1}{A}\frac{dA}{dx} = e\frac{d\phi}{dx} - M_e\left\{\begin{array}{l}\dfrac{\omega_c^2}{\nu_{ei}+\nu_{en}+\alpha_B\omega_c} V_e + \nu_{en}\left(V_e - V_n\right) \\ +\nu_{ei}\left(V_e - V_i\right) + \nu_{ion}\left(V_e - V_n\right) - \nu_{wall} V_e\end{array}\right\} \tag{3}$$

where k is Boltzmann constant, T_e electron temperature, M_e electron mass, V_e axial electron velocity, ω_c electron cyclotron frequency, ν_{ei} electron-ion Coulomb collision frequency, ν_{en} electron-neutral elastic collision frequency, and α_B Bohm diffusion coefficient.

Electron energy:

$$\begin{aligned}&\frac{d}{dx}\left[N_e V_e\left\{\frac{1}{2}M_e\left(V_e^2 + V_{e\theta}^2\right) + \frac{5}{2}kT_e\right\}\right] \\ &+\left[N_e V_e\left\{\frac{1}{2}M_e\left(V_e^2 + V_{e\theta}^2\right) + \frac{5}{2}kT_e\right\}\right]\frac{1}{A}\frac{dA}{dx} \\ &= eN_e V_e \frac{d\phi}{dx} - N_e \nu_{en}\frac{2M_e}{M_n}\frac{3}{2}k\left(T_e - T_n\right) \\ &- N_e \nu_{ei}\frac{2M_e}{M_i}\frac{3}{2}k\left(T_e - T_i\right) - N_e \nu_{ion} E' - N_e \nu_{wallE} E''\end{aligned} \tag{4}$$

where $V_{e\theta}$ is azimuthal electron velocity, M_n neutral mass, T_n neutral temperature, T_i ion temperature, E' electron energy loss of ionization (including excitation), ν_{wallE} frequency of electron energy loss to channel wall, and E" electron energy loss to channel wall.

Azumuthal electron velocity:

$$V_{e\theta} = \frac{\omega_c}{\nu_{ei} + \nu_{en} + \alpha_B \omega_c} V_e = \Omega_e V_e \quad (5)$$

where Ω_e is electron Hall parameter.

Current continuity:

$$eN_e(V_i - V_e)A = J \quad (6)$$

where J is discharge current.

Global mass continuity:

$$(M_n N_n V_n + M_i N_i V_i)A = m \quad (7)$$

where N_n is neutral number density, N_i ion (electron) number density, and m mass flow rate.

We also assume that velocity of neutrals is constant (thermal velocity) and that temperatures of neutrals, ions, the channel wall and secondary electrons emitted from the wall are constant (1000 K).

$$V_n = \text{cons tan t}\left(= \left(\frac{5}{3}\frac{kT_n}{M_n}\right)^{1/2}\right) \quad (8)$$

$$T_n = T_i = T_{wall} = T_{se} = \text{cons tan t}(= 1000\text{K}) \quad (9)$$

where T_{wall} is channel wall temperature, and T_{se} secondary-emission-electron temperature.

At the upstream end (at the anode), the velocity of ions is assumed to be minus magnetosonic velocity because of the sheath criteria, and an electric potential of zero is given.
Upstream boundary conditions:

$$V_i = -\left\{\frac{5}{3}T_e + \frac{2}{3}\frac{M_e}{M_i}(1+\Omega_e^2)V_e^2\right\}^{1/2} \quad (10)$$

$$\phi = 0 \quad (11)$$

The frequency of ion flux loss to channel wall ν_{wall} is determined as follows:

$$\nu_{wall} = \frac{1}{W} \times 2 \times \frac{1}{N_e} \times \Gamma_i \quad (12)$$

$$\Gamma_i = \left(\frac{kT_e}{2\pi M_e}\right)^{1/2} N_e \times \exp\left(\frac{e\phi'}{kT_e}\right) \times (1-\delta) \quad (\phi' \le 0) \quad (13)$$

$$\left(\frac{kT_e}{2\pi M_e}\right)^{1/2} N_e \quad (\phi' \ge 0) \quad (14)$$

where W is channel width, Γ_i ion (electron) flux to channel wall, ϕ ' wall potential on plasma potential, and δ secondary electron emission coefficient.

The frequency of electron energy loss to channel wall ν_{wallE} is determined as follows:

$$\nu_{wallE} E'' = \frac{1}{W} \times 2 \times \frac{1}{N_e} \times \Gamma_e \times E'' \quad (15)$$

$$\Gamma_e \times E'' = \left(\frac{kT_e}{2\pi M_e}\right)^{1/2} N_e \times \exp\left(\frac{e\phi'}{kT_e}\right) \quad (\phi' \le 0) \quad (16)$$

$$\times [(2kT_e - e\phi') - \delta(2kT_{se} - e\phi')]$$

$$\left(\frac{kT_e}{2\pi M_e}\right)^{1/2} N_e \times 2k(T_e - T_{se}) \quad (\phi' \ge 0) \quad (17)$$

where Γ_e is electron flux to channel wall.

Both the wall losses depend on sheath structure in front of acceleration channel wall. The wall potential is determined with the sheath theory with negative potential as follows:

$$\phi' = -\frac{kT_e}{e}\ n\left[(1-\delta)e^{1/2}\frac{\bar{c}_e}{4v_b}\right]$$

$$= -\frac{kT_e}{e}\left[\frac{1}{2} + n\left\{\left(\frac{M_i}{2\pi M_e}\right)^{1/2}(1-\delta)\right\}\right] \quad (18)$$

where $\bar{c}_e$ is electron thermal velocity, and v_b Bohm velocity.

The secondary electron emission coefficient of boron nitride is given as follows.

$$\delta = 0.1983 \times \left(\frac{kT_e(K)}{e}\right)^{0.576} \quad (19)$$

When the emission coefficient is above 0.997 (T_e>16.5 eV), the wall potential becomes positive. Then, the wall losses intensively become large as predicted from Eqs.(14) and (17).

The following popular frequencies of ionization collision, electron-ion Coulomb collision, electron-neutral elastic collision, and Bohm diffusion are used.

Ionization collision frequency:

$$\nu_{ion} = N_n \sigma_{ion}\left(\frac{8kT_e}{\pi M_e}\right)^{1/2}\left(1 + 2\frac{kT_e}{E_i}\right)\exp\left(-\frac{E_i}{kT_e}\right) \quad (20)$$

$\sigma_{ion} = 3.6 \times 10^{-20}(\text{m}^2)$ (Ionization collision cross section)

$E_i = 12.1(\text{eV})$ (Ionization energy of xenon)

$E' = 2.5 \times E_i$ (Electron energy loss of ionization, including excitation)

Electron-ion Coulomb collision frequency:

$$\nu_{ei} = 1.5 \times 10^{-6}\frac{N_e(\text{cm}^{-3})\ n\Lambda}{T_e(\text{eV})^{3/2}} \quad (21)$$

where $n\Lambda$ is Coulomb Logarithm.

Electron-neutral elastic collision frequency:

$$\nu_{en} = N_n \sigma_{en}\left(\frac{8kT_e}{\pi M_e}\right)^{1/2} \quad (22)$$

$\sigma_{en} = 27 \times 10^{-20}(\text{m}^2)$ (Electron-neutral collision cross section)

Bohm diffusion (anomalous diffusion):

$$\alpha_B \omega_c = \alpha_B \times \frac{eB}{M_e} \tag{23}$$

where B is radial magnetic field strength.

After some transformation of Eqs.(1)-(4), the four ordinary differential equations are integrated downstream from the upstream end using the four-order Runge-Kutta method. Numerical integration is carried out with arbitrary values of N_e and T_e at the upstream end; then near a magnetosonic point inside the acceleration channel the integration is stopped, and the zero/zero-condition, i.e., the internal sonic condition, is checked[7],[8]. Iteration is made as changing N_e and T_e. With a near-zero/zero-condition, all subsonic values are connected to supersonic ones with L'Hopital's rule.

An attenuation factor of the present wall losses to the full losses induced from the negative sheath theory, Eqs.(12) and (15), is introduced, and it is 1/100 in this calculation. A Bohm diffusion coefficient is assumed to be 1/75; that is, a popular value of 1/16 is not used considering experimental data.

Experimental and Calculation Results

Operational Characteristics Dependent on Magnetic Field Shape and Strength

Figure 6 shows the characteristics of discharge current, thrust, specific impulse and thrust efficiency dependent on magnetic field strength for the THT-III and THT-IIIA thrusters at a constant discharge voltage of 200 V and a constant mass flow rate of 2 mg/s, in which the radial magnetic field strength represents the maximum near the acceleration channel exit as shown in Fig.4. The discharge current intensively decreases with increasing magnetic field strength to about 130 Gauss although the slope becomes small, and it is almost constant around 150 Gauss. The discharge current for the THT-III thruster abruptly jumps near 160 Gauss, and then it gradually decreases. On the other hand, the operation for the THT-IIIA thruster begins to be unstable around 180 Gauss, although noises of about 15-30 kHz on discharge current waveform due to ionization instability, as shown in Fig.7, disappear above the magnetic field strength. Finally, the discharge current increases to the high value for the THT-III thruster at 250 Gauss[4]-[6]. As a result, the THT-IIIA thruster can be stably operated in the wider range of magnetic field strength. The difference of the discharge current characteristics for the THT-III and THT-IIIA thrusters is expected to be related to that of magnetic field shape; however the physics remains unclear.

The thrust for the THT-III thruster, as shown in Fig.6(b), exhibits little variation with magnetic field strength, and it is almost 23 mN; the specific impulse is around 1160 sec. On the other hand, although the thrust for the THT-IIIA thruster

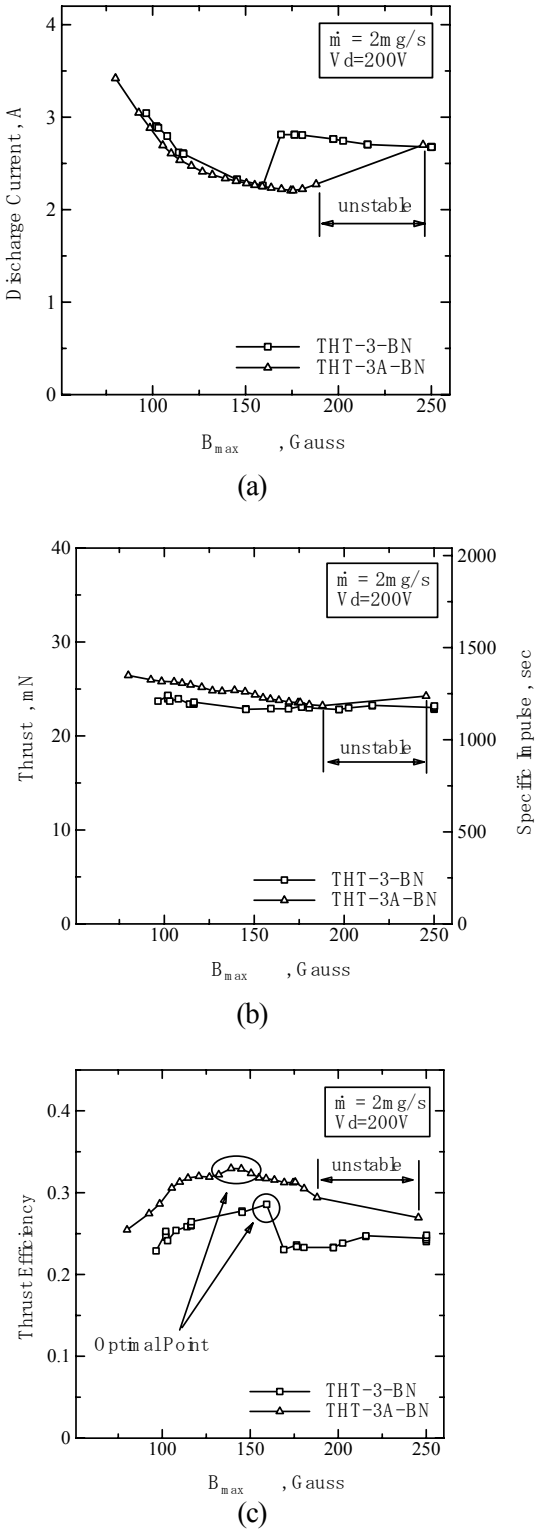

Figure 6 Characteristics of discharge current, thrust, specific impulse and thrust efficiency dependent on magnetic field strength for THT-III and THT-IIIA thrusters at 200 V and 2 mg/s. (a) discharge current; (b) thrust and specific impulse; (c) thrust efficiency.

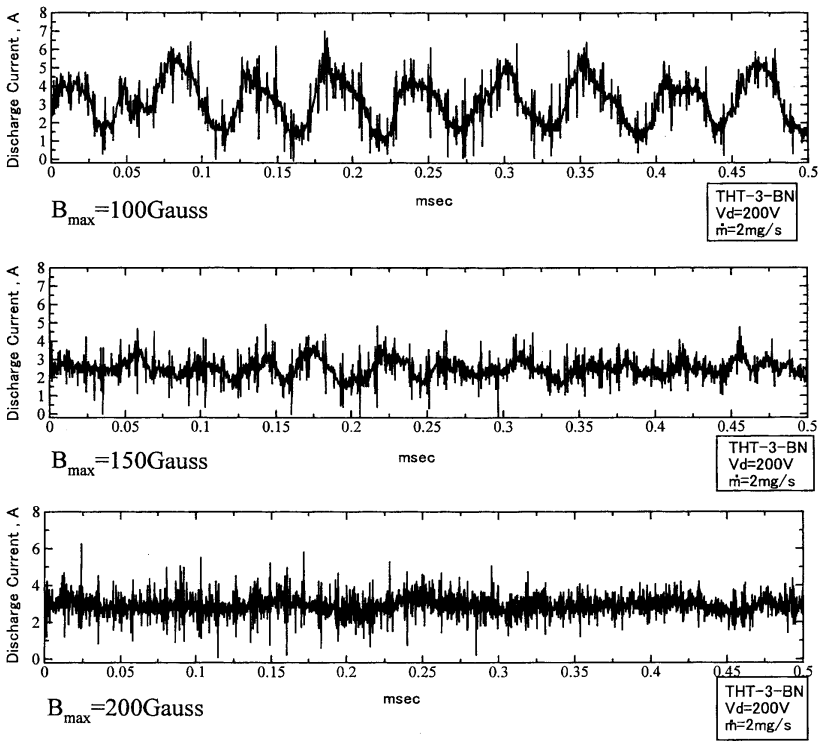

Figure 7 Discharge current waveforms dependent on magnetic field strength for THT-IIIA thruster at 200 V and 2 mg/s.

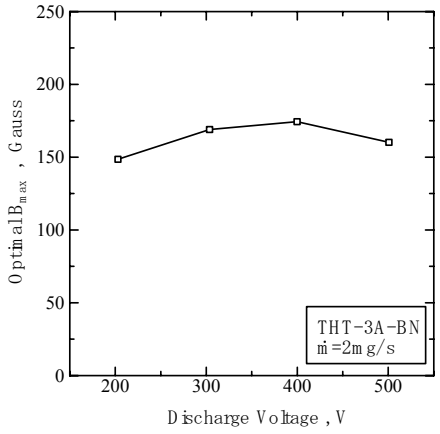

Figure 8 Optimum magnetic field strength vs discharge voltage characteristics for THT-IIIA thruster at 2 mg/s.

gradually decreases with increasing magnetic field strength, it is slightly higher than that for the THT-III thruster below about 180 Gauss. The thrust and the specific impulse for the THT-IIIA thruster are about 25 mN and 1260 sec, respectively, at 150 Gauss. This is explained as follows. For the THT-IIIA thruster, the plasma is generated further downstream inside the acceleration channel compared with that for the THT-III thruster because the magnetic field is intensively concentrated near the channel exit, and then the ions created are efficiently accelerated and exhausted with smaller wall losses.

Accordingly, the thrust efficiency for the THT-IIIA thruster, as shown in Fig.6(c), is higher than that for the THT-III thruster at a constant magnetic field strength. A thrust efficiency of 33 % is achieved at 150 Gauss with the THT-IIIA thruster as compared to 29 % with the THT-III thruster. It is noted that the thrust efficiency characteristics dependent on the discharge current and thrust characteristics have peaks with varying magnetic field strength; that is, there exist an optimum magnetic field strength at a constant discharge voltage and a constant mass flow rate. Figure 8 shows the optimum magnetic field strength vs discharge voltage characteristics for the THT-IIIA thruster at 2 mg/s. It is found that the optimum field strength is a weak function of discharge voltage. They are about 150 Gauss with all discharge voltages.

Figure 9 shows the characteristics of discharge current, thrust, specific impulse and thrust efficiency dependent on discharge voltage for the THT-IIIA thruster at a constant magnetic field strength of 150 Gauss at a constant mass flow rate of 2 mg/s. The discharge current intensively increases with an increase in discharge voltage up to 100 V because of abrupt ionization; then rapidly decreases, and it is almost constant in the wide range of discharge voltage above 150 V

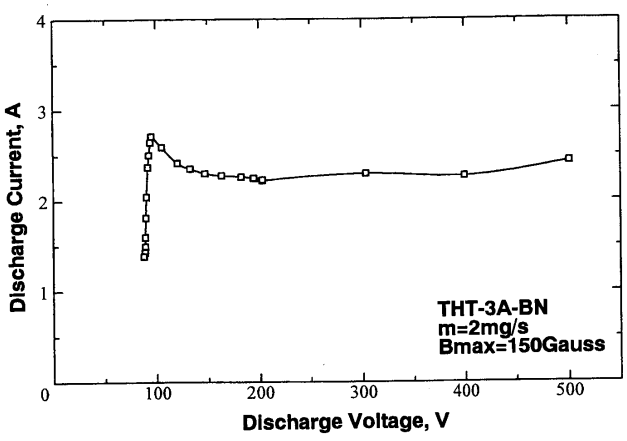

(a)

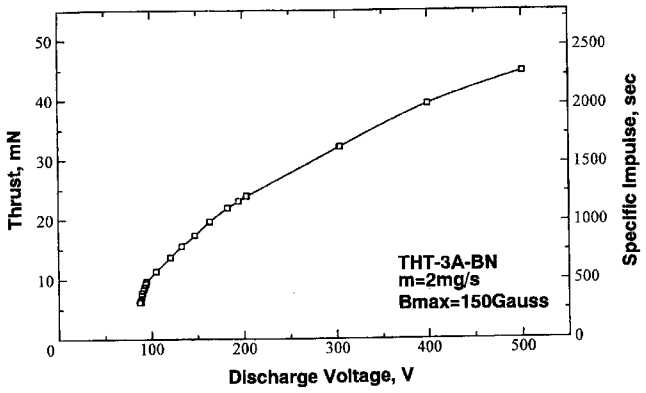

(b)

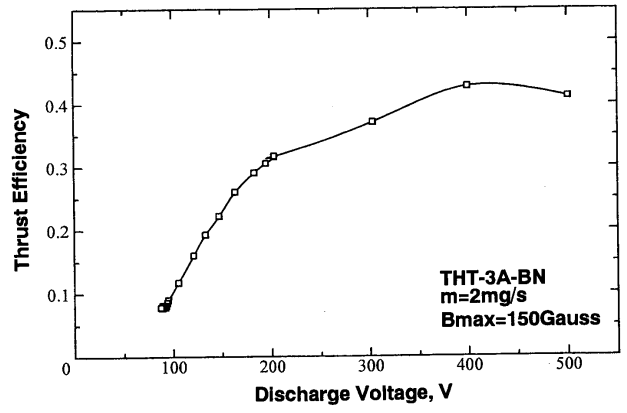

(c)

Figure 9 Characteristics of discharge current, thrust, specific impulse and thrust efficiency dependent on discharge voltage for THT-IIIA thruster at 150 Gauss and 2 mg/s. (a) discharge current; (b) thrust and specific impulse; (c) thrust efficiency.

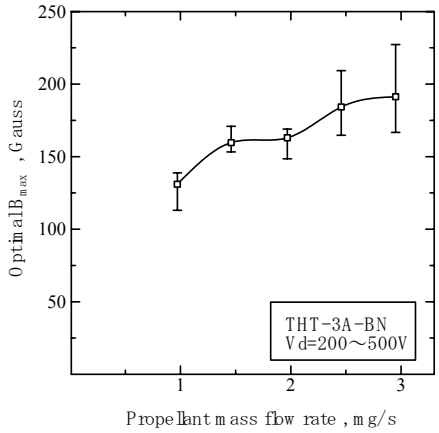

Figure 10 Optimum magnetic field strength vs mass flow rate characteristics for THT-IIIA thruster at 200-500 V.

under fully-ionized conditions. Because the thrust and the specific impulse gradually increase, the thrust efficiency gradually increases. A maximum thrust efficiency of 43 % is achieved at a specific impulse of 2000 sec and a thrust of 39 mN with a discharge voltage of 400 V.

Operational Characteristics Dependent on Propellant Mass Flow Rate

Figure 10 shows the optimum magnetic field strength vs mass flow rate characteristics for the THT-IIIA thruster, in which the optimum values are within an error bar with varying discharge voltage at a constant mass flow rate. The optimum field strength gradually increases with mass flow rate. This is expected because there is an optimum Hall parameter mainly related to electron current conduction.

Figures 11 and 12 show the discharge current, thrust, specific impulse and thrust efficiency characteristics as a function of mass flow rate for the THT-IIIA thruster at optimum

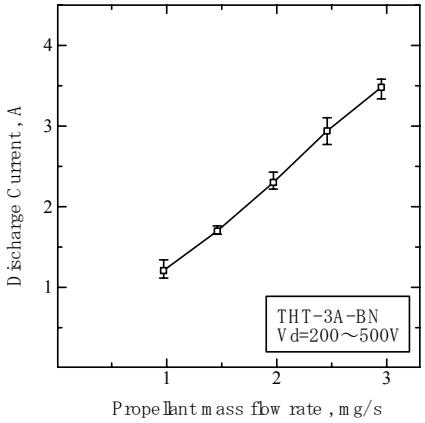

Figure 11 Discharge current vs mass flow rate characteristics for THT-IIIA thruster at optimum magnetic field strengths with 200-500 V.

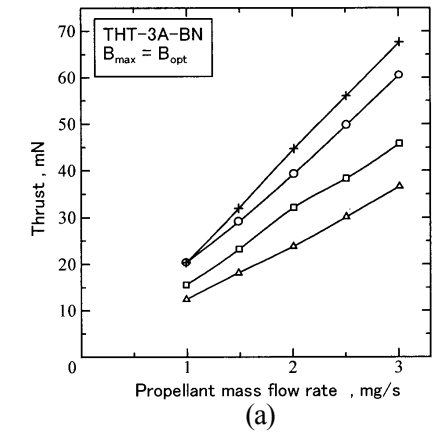

(a)

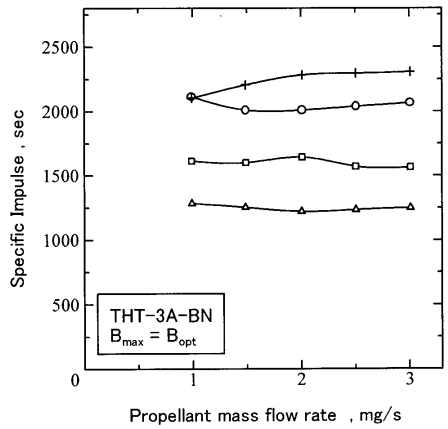

(b)

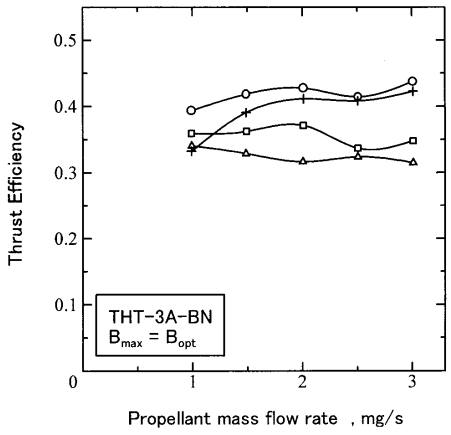

(c)

Vd=200V
Vd=300V
Vd=400V
Vd=500V

Figure 12 Characteristics of thrust, specific impulse and thrust efficiency dependent on mass flow rate for THT-IIIA thruster at optimum magnetic field strengths with 200-500 V. (a) thrust; (b) specific impulse; (c) thrust efficiency.

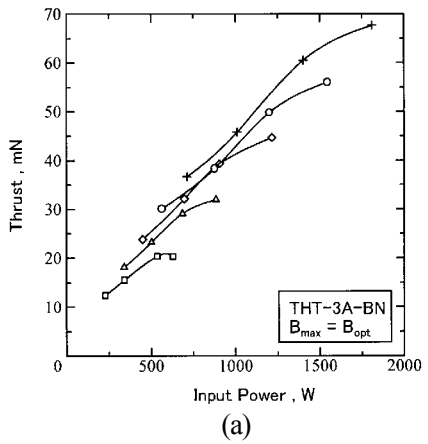

(a)

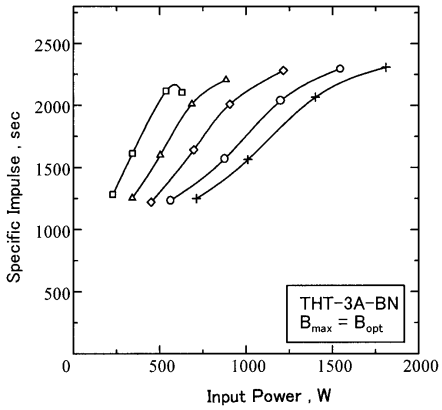

(b)

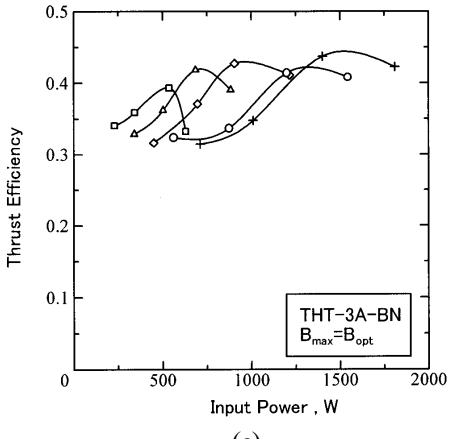

(c)

$\dot{m}$=1mg/s
$\dot{m}$=1.5mg/s
$\dot{m}$=2mg/s
$\dot{m}$=2.5mg/s
$\dot{m}$=3mg/s

Figure 13 Characteristics of thrust, specific impulse and thrust efficiency dependent on input power for THT-IIIA thruster at optimum magnetic field strengths with 1-3 mg/s. (a) thrust; (b) specific impulse; (c) thrust efficiency.

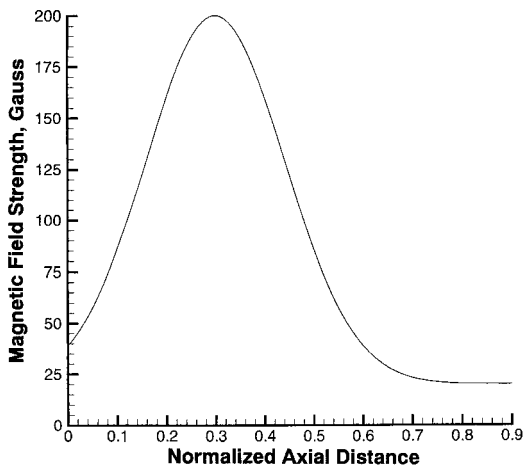

(a)

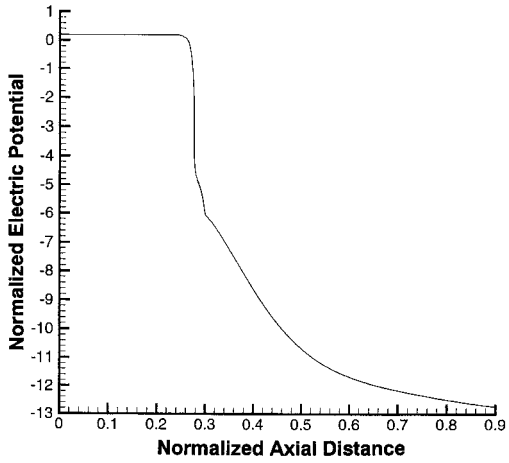

(b)

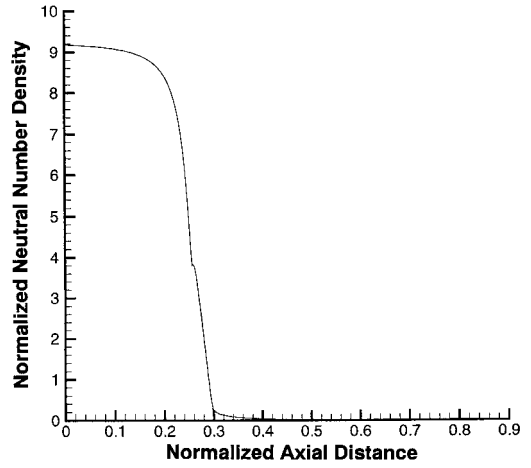

(c)

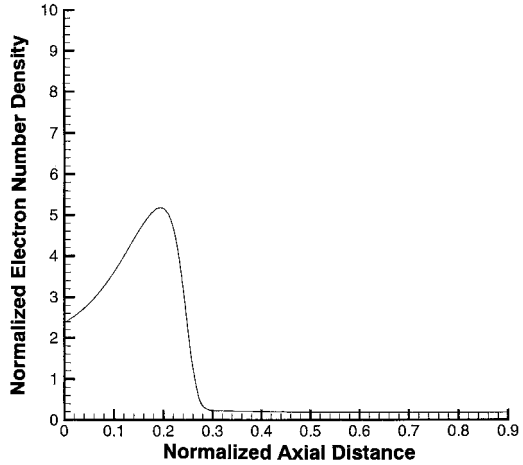

(d)

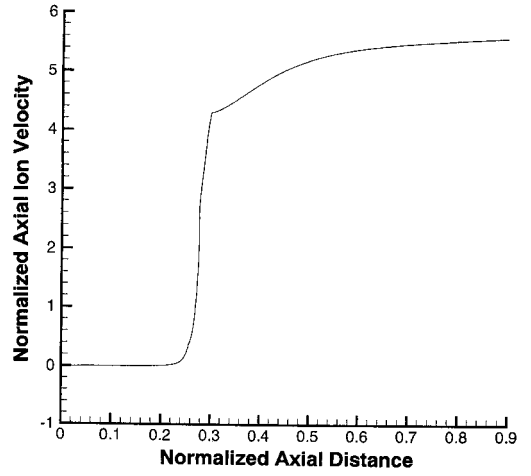

(e)

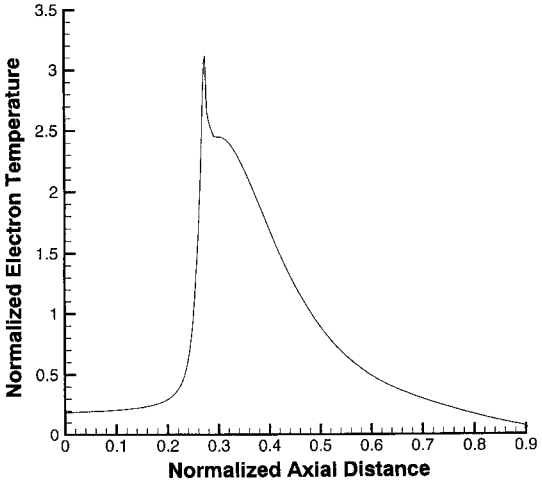

(f)

Figure 14 Calculation of Hall thruster flowfield. (a) magnetic field; (b) electric potential; (c) neutral number density; (d) electron number density; (e) axial ion velocity; (f) electron temperature.

magnetic field strengths. The discharge voltage linearly increases with mass flow rate although it is independent of discharge voltage at a constant mass flow rate. The thrust also linearly increases with mass flow rate, and an increase in discharge voltage raises the thrust at a constant mass flow rate. On the other hand, the specific impulse is almost constant at a constant discharge voltage although it increases with discharge voltage at a constant mass flow rate. Both the thrust and the specific impulse range from 10 to 70 mN and from 1200 to 2300 sec, respectively, in the present operations. Accordingly, the thrust efficiency characteristics have a complicated manner on propellant mass flow rate and discharge voltage, and it ranges from 30 to 45 %.

Operational Characteristics Dependent on Input Power

Figure 13 shows the thrust, specific impulse and thrust efficiency characteristics dependent on input power for the THT-IIIA thruster at optimum magnetic field strengths. The thrust gradually increases with input power at a constant mass flow rate, and then, near high input powers corresponding to high discharge voltages around 500 V, a rate of increase becomes small. The input power at the lowest mass flow rate of 1 mg/s ranges from 250 to 650 W and at the highest mass flow rate of 3mg/s from 750 to 1800 W. The input power range can be drastically changed by varying mass flow rate. Both the specific impulse and the thrust efficiency also increase with input power although they slowly increase or decrease in the high input power range.

Plasma Features and Plasma Acceleration Processes

Figure 14 shows the calculated results of the axial variations of electric potential, neutral number density, electron number density, axial ion velocity and electron temperature, including magnetic field profile. The axial coordinate is normalized with 50 mm, and zero represents the anode position; 0.3 the acceleration channel exit; that is, the channel length is 15 mm. The channel width is 15 mm, and a straight nozzle without wall losses is fitted in the downstream region outside the acceleration channel. The discharge current and the mass flow rate are 1.77 A and 2.0 mg/s, respectively. The number densities of neutrals and electrons are normalized with 9.80×10^{17} m^{-3}, the axial ion velocity with 2.98×10^{3} m/s, and the electron temperature and the electric potential with 12.1 eV (V). The magnetic field shape with a maximum of 200 Gauss is similar to the experimental one.

The neutral number density intensively decreases downstream from an axial position of about 0.2, i.e., from about 0.1 upstream from the acceleration channel exit, with a magnetic field strength of about 150 Gauss; that is, ionization is enhanced. The electron number density has a peak near this location because the ion velocity is zero. For the upstream region, an electron pressure makes plasma diffuse in the direction of the anode; i.e., the upstream region is a diffuse one without an electric field. On the other hand, the ions created in the thin ionization region are intensively accelerated downstream by a high electric field against a reverse electron pressure. The characteristic of electron temperature with a peak of about 36 eV is also reasonable. Consequently, both ionization and acceleration, intensively and efficiently, occur in the thin region with about 3 mm thick near the acceleration channel exit, although the plasma is gradually accelerated outside the channel without losses. The calculated discharge voltage was 157 V; the specific impulse and the thrust efficiency were 1500 sec and 62 %, respectively. When considering the electrode sheath drops, the calculated thruster performance roughly agrees with the experimental ones.

Conclusions

Low-power Hall thruster performance was investigated using THT-III-series Hall thrusters. The discharge current characteristics were sensitive to magnetic field shape and strength. The discharge current gradually decreased with increasing magnetic field strength at a constant mass flow rate; a rate of increase slowly decreased, and then the current almost became constant. Although the thrust was hardly sensitive to magnetic field strength, that for the THT-IIIA thruster with more intensive concentration of magnetic field near the acceleration channel exit, i.e., with a smaller magnetic field at the anode, slightly decreased with increasing magnetic field strength. The THT-IIIA thruster could be stably operated in a wider range of magnetic field strength than that for the THT-III thruster. As a result, for the THT-IIIA thruster, a higher thrust efficiency was achieved with a lower discharge current and a higher thrust for an optimum magnetic field strength regardless of discharge voltage at a constant mass flow rate. Accordingly, both the thrust and the specific impulse ranged from 10 to 70 mN and from 1200 to 2300 sec, respectively, at discharge voltages of 200-500 V with mass flow rates of 1-3 mg/s in a wide input power range of 250-1800 W. The thrust efficiency ranged from 30 to 45 %. Furthermore, one-dimensional Hall thruster flowfield calculation was made to understand the inner physical phenomena. Both ionization and acceleration were found to, intensively and efficiently, occur in a thin region with a few mm thick near the acceleration channel exit. The calculated thruster performance roughly agreed with the experimental ones.

Acknowledgments

Hirokazu Tahara would like to thank Manuel Martinez-Sanchez, Department of Aeronautics and Astronautics, Massachusetts Institute of Technology (MIT), who provided lots of significant comments for Hall thruster research and development during stay at MIT, March to November 2000. The authors would also like to thank

Eduardo Ahedo, E.T.S.I. Aeronautics, Universidad Politecnica de Madrid, who provided useful advices for Hall thruster flowfield calculation.

References

[1] Kim, V.," Main Physical Features and Processes Determining the Performance of Stationary Plasma Thrusters," *Journal of Propulsion and Power*, Vol.14, 1998, pp.736-743.

[2] Stephenson, R.R.," Electric Propulsion Development and Application in the United States," *Proceedings of the 24th International Electric Propulsion Conference, Moscow*, Vol.1, 1995, Paper No. IEPC 95-1, pp.1-12.

[3] Zhurin, V.V., Kaufman, H.R., and Robinson, R.S.," Physics of Closed Drift Thrusters," *Proceedings of the 25th International Electric Propulsion Conference, Cleveland*, Vol.2, 1997, Paper No. IEPC 97-191, pp.1175-1182.

[4] Tahara, H., Nikai, Y., Yasui, T., and Yoshikawa, T.," Hall Thruster Research at Osaka University," 35th AIAA/ASME/SAE/ASEE Joint Propulsion Conference and Exhibit, Los Angeles, 1999, AIAA Paper No. 99-2570.

[5] Goto, D., Tahara, H., Nikai, Y., Yasui, T., and Yoshikawa, T.," Research and Development of Hall Effect Thrusters at Osaka University," *Proceedings of the 26th International Electric Propulsion Conference, Kitakyushu*, Vol.1, 1999, Paper No. IEPC 99-121, pp.675-682.

[6] Tahara, H., Mitsuo, K., Goto, D., Yasui, T., and Yoshikawa, T.," Operating Characteristics of Low Power Hall Thrusters," 22nd International Symposium on Space Technology and Science, Morioka, 2000, Paper No. ISTS 2000-b-36p.

[7] Ahedo, E., and Martinez-Sanchez, M.," One-Dimensional Plasma Structure in Hall Thrusters," 34th AIAA/ASME/SAE/ASEE Joint Propulsion Conference and Exhibit, Cleveland, 1998, AIAA Paper No. 98-8788.

[8] Ahedo, E., Martinez, P., and Martinez-Sanchez, M.," Steady and Linearly-Unsteady Analysis of a Hall Thruster with an Internal Sonic Point," 36th AIAA/ASME/SAE/ASEE Joint Propulsion Conference and Exhibit, Huntsville, 2000, AIAA Paper No. 2000-3655.